Ablation of cholesterol biosynthesis in neural stem cells increases their VEGF expression and angiogenesis but causes neuron apoptosis

Kanako Saito[a,b,1], Veronique Dubreuil[a,1,2], Yoko Arai[a], Michaela Wilsch-Bräuninger[a], Dominik Schwudke[a,3], Gesine Saher[c], Takaki Miyata[b], Georg Breier[d], Christoph Thiele[a], Andrej Shevchenko[a], Klaus-Armin Nave[c], and Wieland B. Huttner[a,4]

[a]Max Planck Institute of Molecular Cell Biology and Genetics, D-01307 Dresden, Germany; [b]Nagoya University Graduate School of Medicine, Nagoya, Aichi 466-8550, Japan; [c]Max Planck Institute of Experimental Medicine, D-37075 Göttingen, Germany; and [d]Institute of Pathology, Medical Faculty, Dresden University of Technology, D-01307 Dresden, Germany

Communicated by Kai Simons, Max Planck Institute of Molecular Cell Biology and Genetics, Dresden, Germany, April 1, 2009 (received for review February 10, 2009)

Although sufficient cholesterol supply is known to be crucial for neurons in the developing mammalian brain, the cholesterol requirement of neural stem and progenitor cells in the embryonic central nervous system has not been addressed. Here we have conditionally ablated the activity of squalene synthase (SQS), a key enzyme for endogenous cholesterol production, in the neural stem and progenitor cells of the ventricular zone (VZ) of the embryonic mouse brain. Mutant embryos exhibited a reduced brain size due to the atrophy of the neuronal layers, and died at birth. Analyses of the E11.5–E15.5 dorsal telencephalon and diencephalon revealed that this atrophy was due to massive apoptosis of newborn neurons, implying that this progeny of the SQS-ablated neural stem and progenitor cells was dependent on endogenous cholesterol biosynthesis for survival. Interestingly, the neural stem and progenitor cells of the VZ, the primary target of SQS inactivation, did not undergo significant apoptosis. Instead, vascular endothelial growth factor (VEGF) expression in these cells was strongly upregulated via a hypoxia-inducible factor-1–independent pathway, and angiogenesis in the VZ was increased. Consistent with an increased supply of lipoproteins to these cells, the level of lipid droplets containing triacylglycerides with unsaturated fatty acyl chains was found to be elevated. Our study establishes a direct link between intracellular cholesterol levels, VEGF expression, and angiogenesis. Moreover, our data reveal a hitherto unknown compensatory process by which the neural stem and progenitor cells of the developing mammalian brain evade the detrimental consequences of impaired endogenous cholesterol biosynthesis.

lipid droplets | mass spectrometry | neuroepithelial cells | neurogenesis | radial glia

Cholesterol is a key lipid constituent of post-Golgi membranes of mammalian cells, notably the plasma membrane. Together with sphingolipids, cholesterol forms lateral membrane lipid assemblies called "lipid rafts" that interact with "raftophilic" membrane proteins to generate specific cholesterol-based membrane microdomains. The latter have important roles in cell functions, such as membrane traffic and signal transduction (1–3).

Not surprisingly in light of their highly elaborate morphology, neurons have been shown to possess distinct cholesterol-based plasma membrane microdomains (4–7). Accordingly, neuronal differentiation, in particular synaptogenesis, is a cholesterol-dependent process (8, 9). However, the cholesterol requirement of the neural stem and progenitor cells that give rise to neurons during the development of the mammalian CNS is unclear.

There are various reasons to suspect that neural stem and progenitor cells may be sensitive to a lack of cholesterol. Interference with cholesterol biosynthesis leads to massive defects in CNS development that appear even before the onset of neurogenesis (10). Moreover, an apical plasma membrane protein of the neural stem and progenitor cells lining the lumen of the neural tube [i.e., the ventricular zone (VZ) progenitors], prominin-1 (CD133) (11), directly interacts with membrane cholesterol and is a key constituent of a cholesterol-based plasma membrane microdomain (12). These microdomains are released from VZ progenitor cell-surface protrusions as membrane vesicles into the neural tube fluid, a developmentally regulated process that is promoted by cholesterol depletion (13–15).

Like other cells, VZ progenitor cells as well as the neurons derived therefrom have 2 principal sources of cholesterol: endogenous biosynthesis and external supply. Here we have conditionally ablated cholesterol biosynthesis in VZ progenitors of the mouse embryo and investigated the consequences for brain development. Surprisingly, we find that VZ progenitors protect themselves against cholesterol deprivation by upregulating the expression of VEGF, thereby raising their supply with cholesterol via increased angiogenesis in the VZ, whereas newborn neurons derived from the VZ progenitors undergo apoptosis, resulting in a smaller brain and lethality at birth.

Results

Conditional *SQS* Ablation in VZ Progenitors Using *nestin*-Cre Results in Reduced Size and Altered Structure of the Embryonic Mouse Brain. To specifically ablate cholesterol biosynthesis, we focused on squalene synthase (SQS, also called Fdft1), the enzyme catalyzing the first metabolic step in the cholesterol biosynthetic pathway that is exclusively committed to sterol biosynthesis. A mouse line carrying a floxed *SQS* allele (16) allows the Cre-mediated deletion of exon 5, which encodes the catalytic center. To selectively ablate cholesterol biosynthesis in the neural stem and progenitor cells of the VZ, we crossed $SQS^{flox/flox}$ mice with a transgenic mouse line expressing the Cre recombinase under the control of the rat nestin promoter and enhancer (17), which is known to mediate deletion of floxed genes in VZ progenitors of the developing brain as early as embryonic day 10.5 (E10.5) (18) (see also Fig. 3*A* below). The resulting, conditionally *SQS*-ablated (*SQS*-cKO) embryos and newborn pups

Author contributions: K.S., V.D., G.B., C.T., A.S., and W.H. designed research; K.S., V.D., Y.A., M.W.-B., and D.S. performed research; G.S. and K.-A.N. contributed new reagents/analytic tools; K.S., V.D., Y.A., M.W.-B., D.S., T.M., A.S., and W.H. analyzed data; and K.S., V.D., and W.H. wrote the paper.

The authors declare no conflict of interest.

[1]K.S. and V.D. contributed equally to this article.

[2]Present address: Département de Biologie, Ecole Normale Supérieure, Centre National de la Recherche Scientifique, Unité Mixte de Recherche 8542, 75005 Paris, France.

[3]Present address: National Center for Biological Science, Bangalore, India.

[4]To whom correspondence should be addressed. E-mail: huttner@mpi-cbg.de.

This article contains supporting information online at www.pnas.org/cgi/content/full/0903541106/DCSupplemental.

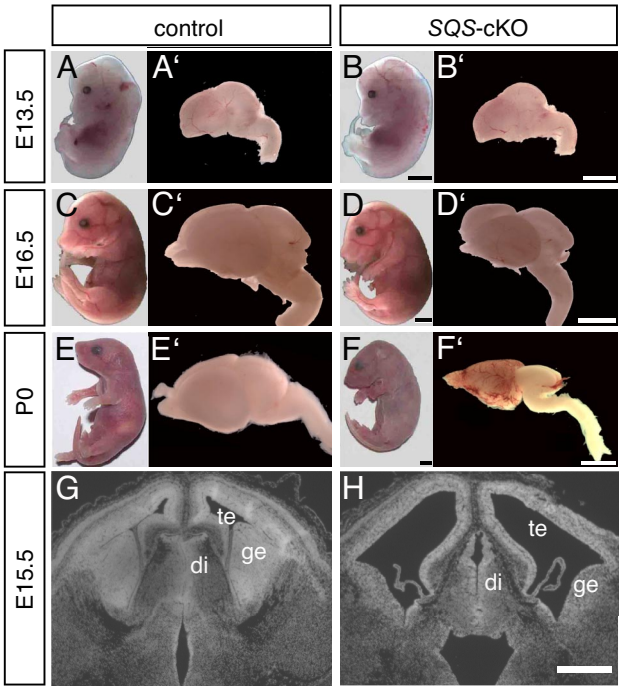

Fig. 1. *SQS* cKO in VZ progenitors using *nestin*-Cre results in reduced size and altered structure of the embryonic mouse brain. (*A–F*) Whole embryos and pups, (*A′–F′*) dissected brains (*E′*, perfused; *F′*, unperfused), and (*G* and *H*) DAPI-stained coronal cryosections through the brain of control (*A*, *A′*, *C*, *C′*, *E*, *E′*, and *G*) and conditionally *SQS*-ablated (*SQS*-cKO) mice using *nestin*-Cre (*B*, *B′*, *D*, *D′*, *F*, *F′*, and *H*) at E13.5–E16.5 and at birth (P0), as indicated. te, dTE; ge, ganglionic eminence; di, DiE. Note that all *SQS*-cKO pups died at birth (hence, no perfusion in *F′*). (Scale bar, 2 mm in *A–F*, 500 μm in *G* and *H*.)

(*SQS*$^{flox/flox}$/*nestin-Cre*$^{+/-}$) were obtained with normal Mendelian frequency [supporting information (SI) Table S1]. However, mutant pups died at birth (postnatal day 0, P0), without their lungs becoming inflated (data not shown), indicating their inability to breathe. Gross morphology of the *SQS*-cKO embryos and newborn pups was similar to that of control littermates (Fig. 1 *A–F*). However, at E16.5 and at P0, the dissected brains of *SQS*-cKO mice exhibited an overt reduction in size when compared with control littermates, which was not yet obvious at E13.5 (Fig. 1 *A'–F'*).

Nonetheless, as early as E13.5 the *SQS*-cKO brain showed subtle changes in structure when examined by DAPI staining of coronal cryosections. The most noticeable defect was a reduction in the radial thickness of the diencephalon (DiE) (data not shown). At E15.5 the *SQS*-cKO brain showed additional structural alterations, notably in the telencephalon, where a reduction in the size of the ganglionic eminences and in the radial thickness of the cortical wall was observed (Fig. 1 *G* and *H*).

SQS Inactivation in VZ Progenitors Results in Apoptosis Predominantly of Young Neurons. We next investigated the reason underlying the reduction in the radial thickness of the cortical wall and DiE. To distinguish between the progenitor-containing and the neuron-enriched layers, we performed immunostaining for β-III-tubulin (TUJ1), a marker of young neurons (19). This revealed a reduction in the radial thickness of the neuronal layers (NL) that was detectable for the DiE at E13.5 but not yet at E12.5, and for the dorsal telencephalon (dTE) at E15.5 but not yet at E13.5 (Fig. 2 *A*, green, and *B*, green columns). We did not observe a significant alteration in the radial thickness of the progenitor-containing layers at any of the stages analyzed (Fig. 2 *A* and *B*, blue columns).

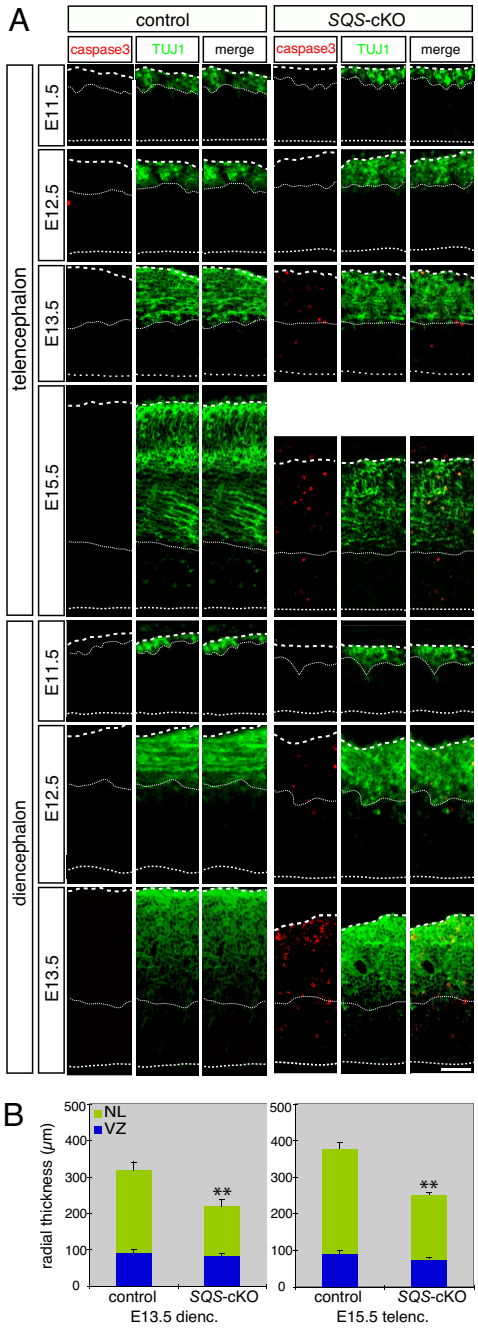

Fig. 2. SQS inactivation in VZ progenitors results in apoptosis predominantly of young neurons. (*A*) Double immunofluorescence for activated caspase3 (red) and β-III-tubulin (TUJ1, green) in coronal cryosections of E11.5–E15.5 dTE and E11.5–E13.5 DiE of control and *SQS*-cKO mice. Lower dotted lines, apical surface; middle dotted lines, boundaries between the VZ (and, when present, SVZ) and the NL; upper dotted lines, basal lamina. Note the predominant occurrence of apoptotic cells in the NL of *SQS*-cKO mice. Each pair of control and *SQS*-cKO immunofluorescence are equal exposures. (Scale bar, 50 μm.) (*B*) Quantification of radial thickness of VZ (blue segment of columns) and NL (green segment of columns) of E13.5 DiE (dienc.) and E15.5 dTE (telenc.) of control and *SQS*-cKO mice. Data are the mean of 4 (dTE) and 5 (DiE) embryos each. Error bars indicate SEM; **, $P < 0.01$.

Given the reduction in radial thickness of the NL without a change in the thickness of the progenitor layers, we investigated whether the former reflected apoptosis of neurons. Both TUNEL staining (data not shown) and immunostaining for

NEUROSCIENCE

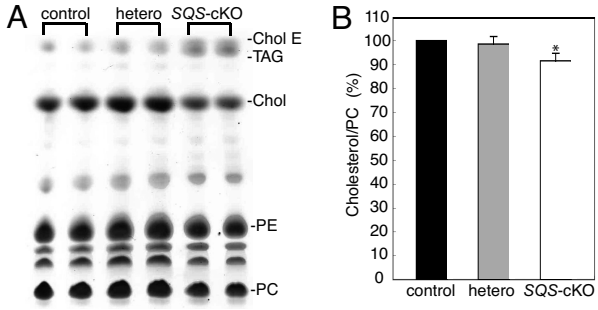

Fig. 3. Comparison of cholesterol levels in control and *SQS*-cKO brain. (*A*) TLC of lipids extracted from a pool of dTE plus DiE of E13.5 control, heterozygous, and *SQS*-cKO mice. Each lane shows the extract of a different embryo. Chol E, cholesterol ester; Chol, cholesterol; PE, phosphatidyl-ethanolamine. The origin (not shown) is beneath the PC spot, and the solvent front is above the Chol E spot. (*B*) Quantification of cholesterol levels after TLC. Data are the mean of 4 independent TLCs, each analyzing 2 different embryos each. For each TLC, the amount of cholesterol in 1 embryo was first determined relative to that of PC, the mean of the resulting values for the 2 embryos was calculated, and this mean value for *SQS*-cKO and heterozygous tissue was expressed as percentage of control tissue. Error bars indicate SEM; *, $P < 0.05$.

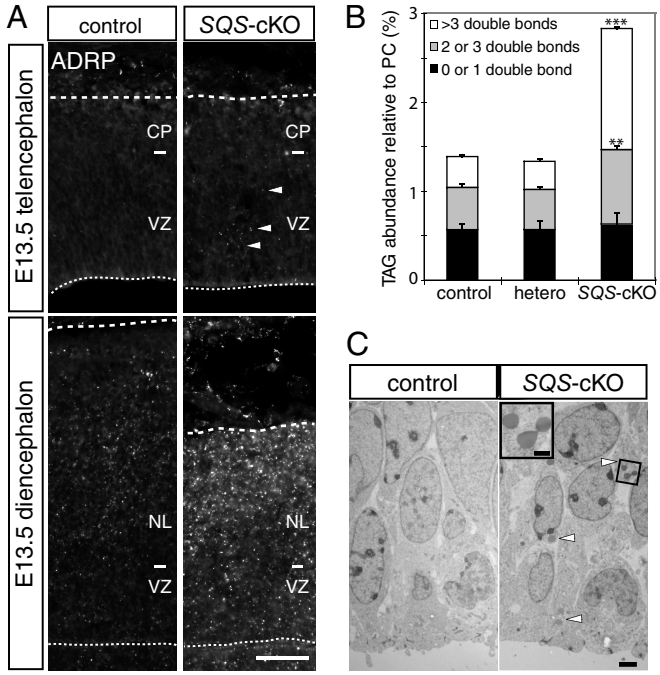

Fig. 4. Increase in lipid droplets and unsaturated TAGs in the *SQS*-cKO embryonic brain. (*A*) Immunofluorescence for ADRP in coronal cryosections of E13.5 dTE (*Top*) and DiE (*Bottom*) of control and *SQS*-cKO mice. Lower dotted lines, apical surface; upper dotted lines, basal lamina; CP, cortical plate; small white bars, boundaries between the VZ (and, when present, SVZ) and the NL; arrowheads indicate lipid droplets in the VZ of the *SQS*-cKO E13.5 dTE. (Scale bar, 50 μm.) (*B*) Quantification of TAG levels as determined by mass spectrometry, expressed as a percentage relative to the PC level. Black segments, TAGs with no or 1 double bond; gray segments, TAGs with 2 or 3 double bonds; white segments, TAGs with more than 3 double bonds (for TAG species, see Table S2). Data are the mean of 3 different embryos each, with each embryo being analyzed in duplicate. Error bars indicate SEM; **, $P < 0.01$; ***, $P < 0.001$. (*C*) EM of VZ progenitors in the E13.5 DiE of control and *SQS*-cKO mice. Apical surface is down. Arrowheads indicate lipid droplets. The area indicated by the square box (*Right*) is shown at higher magnification in the *Inset*. [Scale bars, 2 μm and 500 nm (*Inset*).]

activated caspase-3 (Fig. 2*A*, red), 2 indicators of apoptosis (20), showed that this was indeed the case. Whereas very few, if any, apoptotic cells could be detected in the control brain tissue at any of the stages analyzed, such cells were frequently observed in the *SQS*-cKO dTE at E13.5 and even more so at E15.5, and in the *SQS*-cKO DiE at E12.5 and, massively, at E13.5. Most of the apoptotic cells were found in the NL and only a minor proportion of them in the progenitor layers (Fig. 2*A*, red). We did not observe any significant decrease in ventricular and abventricular mitotic (phosphohistone 3–positive) cells in the *SQS*-cKO E13.5 dTE and DiE (data not shown). We therefore conclude that the reduction in radial thickness of the NL in the *SQS*-cKO E15.5 dTE and E13.5 DiE primarily reflected apoptosis of newborn neurons rather than impaired neurogenesis.

Immunostaining for nestin, a marker of VZ progenitors (i.e., neuroepithelial cells and radial glial cells) (21), revealed a similar pattern for control and *SQS*-cKO E13.5 dTE and DiE, with radial fibers extending all of the way to the basal lamina (Fig. S2). This, together with the unaltered thickness of the progenitor layers and the apoptosis predominantly in the NL (Fig. 2), was consistent with the notion that newborn neurons rather than neural progenitors were affected by the conditional SQS inactivation.

Full-Length SQS Protein Levels in the Embryonic Brain Are Reduced Upon Conditional Ablation of *SQS* Exon 5. Given that the primary target cells for conditional ablation (cKO) of the *SQS* exon 5 by *nestin*-Cre were the VZ progenitors, the preferential apoptosis of newborn neurons (Fig. 2) called for a verification of this ablation and for an analysis of the SQS protein levels in progenitors vs. neurons. As described in detail in *SI Text*, analysis of the E13.5 dTE and DiE revealed that the specific *nestin*-Cre expression in the VZ (Fig. S1*A*) indeed resulted in (*i*) the ablation of SQS exon 5, as revealed by genomic PCR (Fig. S1*B*, *a*); (*ii*) the dramatic reduction in the full-length, exon 5–containing *SQS* mRNA, as revealed by RT-PCR (Fig. S1*B*, *b*); (*iii*) a massive decrease in the full-length SQS protein, as revealed by immunoblotting (Fig. S1*B*, *c* and *d*); and (*iv*) a marked reduction of SQS immunoreactivity in the VZ and, although to a lesser extent, in the NL, as revealed by immunofluorescence (Fig. S1*C*). In fact, the level of SQS immunoreactivity in neurons was found to be higher than that in VZ progenitors (Fig. S1*C*). Thus, the cells in which SQS levels were most reduced (i.e., the VZ progenitors) were largely protected from apoptosis, whereas their progeny, the neurons, was not.

Cholesterol Level in *SQS*-cKO Embryonic Brain Is Only Mildly Reduced. We next investigated the consequences of *SQS* cKO for brain cholesterol levels, that is, the sum of endogenously synthesized cholesterol and that taken up from external sources, such as the ventricular fluid (22) and the blood. Total lipids including cholesterol were extracted from a pool of E13.5 dTE plus DiE and analyzed by TLC and mass spectrometry (see further below). *SQS*-cKO brain tissue showed a small but significant decrease in the ratio of cholesterol over phosphatidylcholine compared with control (Fig. 3 *A* and *B*).

Lipid Droplets Containing Triacylglycerides with Unsaturated Fatty Acyl Chains Are Enriched in *SQS*-cKO Embryonic Brain. Concomitant with the decrease in cholesterol, TLC revealed an increase in triacylglycerides (TAGs), and perhaps in cholesterol esters, in *SQS*-cKO brain tissue (Fig. 3*A*). TAGs and cholesterol esters are known to be stored intracellularly in lipid droplets (23–26). Immunofluorescence for adipocyte differentiation-related protein (ADRP), a lipid droplet marker (27), showed an increase in lipid droplets in both the progenitor layers and NL of E13.5 *SQS*-cKO brain tissue compared with control, which was particularly striking for the DiE (Fig. 4*A*). On conventional EM

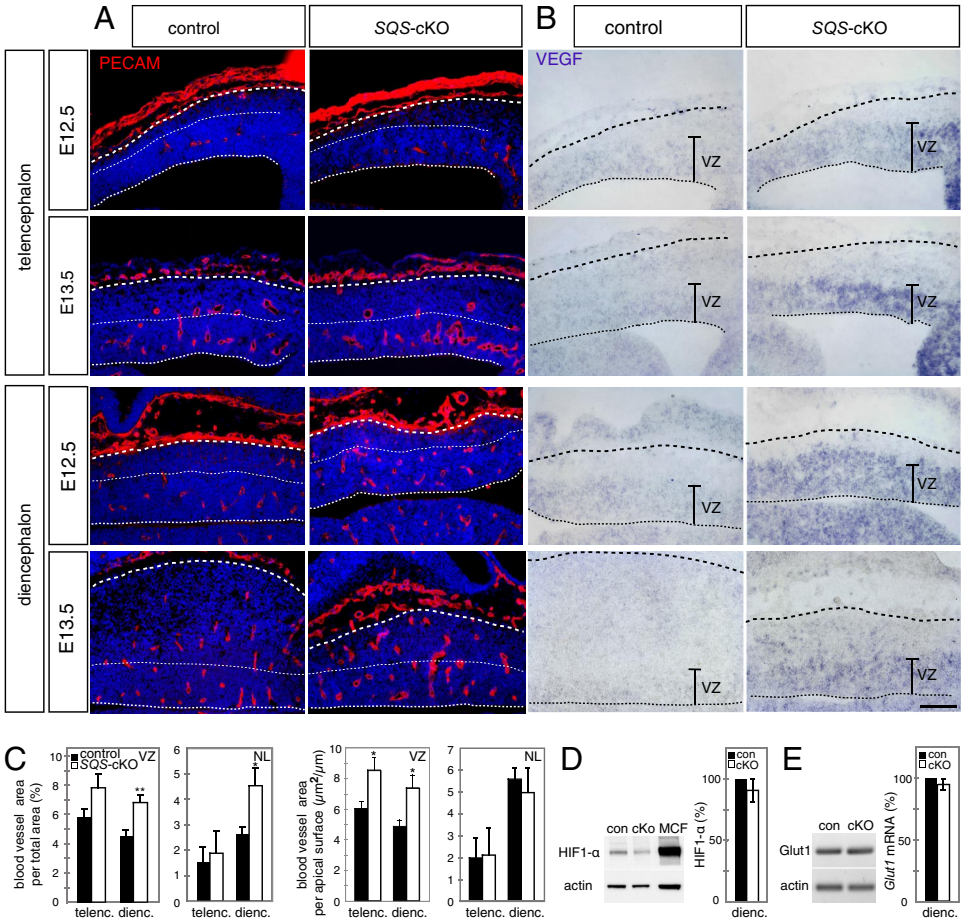

Fig. 5. SQS inactivation in VZ progenitors induces VEGF expression in the VZ, resulting in increased angiogenesis. (*A*) Immunofluorescence for PECAM-1 (red) and DAPI staining (blue) in coronal cryosections of E12.5–E13.5 dTE and DiE of control and *SQS*-cKO mice. Lower dotted lines, apical surface; middle dotted lines, boundaries between the VZ (and, when present, SVZ) and the NL; upper dotted lines, basal lamina. Each pair of control and *SQS*-cKO immunofluorescence are equal exposures. (*B*) In situ hybridization for *VEGF* mRNA in coronal cryosections of E12.5–E13.5 dTE and DiE of control and *SQS*-cKO mice. Lower dotted lines, apical surface; upper dotted lines, basal lamina. The vertical bars indicate the thickness of the VZ. Each pair of control and *SQS*-cKO in situ hybridization are equal exposures. (Scale bar, 100 μm.) (*C*) Quantification of the area occupied by blood vessels as revealed by PECAM-1 immunofluorescence in the E13.5 dTE (telenc.) and DiE (dienc.) of control and *SQS*-cKO mice (see *A*). Blood vessel area in the VZ and NL is expressed either as percentage of the total VZ and NL area, respectively (*Left* and *Middle Left*) or relative to the ventricular (apical) surface (*Right* and *Middle Right*). Data are the mean of 5 embryos each. Error bars indicate SEM; *, $P < 0.05$; **, $P < 0.01$. (*D* and *E*) Immunoblotting of a nuclear fraction for HIF-1α (*D*) and RT-PCR of *Glut1* mRNA (*E*), both obtained from E13.5 DiE (dienc.) of control (con) and *SQS*-cKO (cKO) mice. (*D*, *Left*) Representative immunoblot showing the 120-kDa HIF-1α band and β-actin analyzed as a control for equal protein loading (10 μg total protein per control and *SQS*-cKO lane); MCF, lysate of hypoxia-treated MCF-7 cells loaded as positive control. (*D*, *Right*) Quantification of HIF-1α immunoreactivity. Data are the mean of 2 immunoblots, each analyzing a different embryo. For each immunoblot, HIF-1α immunoreactivity was first determined relative to that of β-actin, and the resulting value for *SQS*-cKO tissue was expressed as percentage of that for control tissue. (*E*, *Left*) Representative RT-PCR of *Glut1* mRNA showing the 458-bp PCR product and the 350-bp β-*actin* PCR product used as internal standard. (*E*, *Right*) Quantification of *Glut1* RT-PCR. Data are the mean of 2 RT-PCRs, each using RNA from a different embryo. For each RT-PCR, the abundance of the *Glut1* PCR product was first determined relative to that of β-*actin*, and the resulting value for *SQS*-cKO tissue was expressed as percentage of that for control tissue. Error bars indicate the variation of the individual values from the mean.

analysis, these lipid droplets were found to be unusually osmiophilic (Fig. 4*C*), suggestive of an abundance of carbon double bonds (28).

Indeed, the analysis of total lipid extracts by shotgun mass spectrometry showed that the amount of total TAGs relative to the total content of phosphatidylcholines (PCs) was increased 2-fold in the pool of *SQS*-cKO E13.5 dTE plus DiE as compared with control (Fig. 4*B*). Interestingly, this was largely due to an increase in the abundance of TAG species with unsaturated fatty acyl moieties, in particular those with more than 3 double bonds per TAG molecule (Fig. 4*B*, Fig. S3, and Table S2). In addition, mass spectrometry corroborated the small reduction in cholesterol and the increase in cholesterol esters observed by TLC (Fig. S3).

***SQS*-Ablated VZ Progenitors Induce VEGF Expression, Resulting in Increased Angiogenesis.** The greater abundance of lipid droplets in the *SQS*-cKO brain tissue raised the possibility that the lack of cholesterol biosynthesis in VZ progenitors and the neurons derived therefrom upon *SQS* exon 5 cKO was compensated by increased uptake of lipoproteins carrying cholesterol and other lipids. VZ progenitors, which were found to be much less susceptible to the *SQS*-cKO–induced apoptosis than neurons (Fig. 2*A*), line the ventricular lumen (in contrast to neurons), which is known to contain lipoproteins (22). We therefore explored such a possible compensation by immunostaining for megalin, low-density lipoprotein receptor-related protein known to be expressed at the ventricular surface of VZ progenitors (29–31). However, megalin immunoreactivity, which showed the

NEUROSCIENCE

characteristic concentration at the ventricular side of the VZ, did not seem to be strikingly different in abundance in the *SQS*-cKO E13.5 dTE and DiE when compared with the control (data not shown).

Another possible way of compensating for the lack of cholesterol biosynthesis would be increased lipoprotein uptake from the blood. We therefore examined the blood vessels in the E12.5 and E13.5 control and *SQS*-cKO brain by immunostaining for platelet endothelial cell adhesion molecule-1 (PECAM-1), a membrane protein found at the surface of endothelial cells (32). This showed that *SQS* cKO resulted in an increase in blood vessels, which was most obvious for the E13.5 DiE (Fig. 5*A*). Specifically, quantification on cryosections revealed an increase, in the E13.5 *SQS*-cKO dTE and DiE as compared with control, in the VZ area occupied by PECAM-1–stained blood vessels. This increase was observed irrespective of whether blood vessel area in the VZ was expressed per total VZ area (Fig. 5*C*, *Left*) or per ventricular (apical) surface (Fig. 5*C*, *Middle Right*). By contrast, the E13.5 *SQS*-cKO dTE and DiE did not exhibit an increase, relative to control brain, in the blood vessel area in the NL when expressed per ventricular (apical) surface (Fig. 5*C*, *Right*). We did observe an increase in blood vessel area in the NL of the E13.5 *SQS*-cKO DiE compared with control when expressed per total NL area (Fig. 5*C*, *Middle Left*), but this increase reflected the reduced thickness of the NL upon *SQS* cKO (Fig. 5*A*, see also Fig. 2) rather than a true increase in angiogenesis.

To explore the underlying cause of the increase in blood vessels in the *SQS*-cKO brain, we performed in situ hybridization for VEGF mRNA, the main angiogenic factor in the developing brain (33–35). Remarkably, we observed a marked increase in *VEGF* mRNA expression in the E12.5 and E13.5 *SQS*-cKO dTE and DiE, which was largely confined to VZ (Fig. 5*B*). On immunostaining for VEGF protein, whereas very little, if any, immunoreactivity could be detected in the E13.5 control DiE, we observed an increased VEGF immunoreactivity in the E13.5 *SQS*-cKO DiE (Fig. S4). This VEGF immunostaining, consistent with the results of in situ hybridization (Fig. 5*B*) and previous observations at earlier developmental stages (36), was predominantly detected in the VZ (Fig. S4). We conclude that cKO of cholesterol biosynthesis in VZ progenitors causes an upregulation of VEGF expression in these cells, which presumably underlies the increased angiogenesis observed primarily in the VZ.

Increased VEGF Expression in *SQS*-Ablated VZ Progenitors Occurs via a HIF-1–Independent Pathway. To further address the molecular mechanism underlying the upregulation of VEGF expression in VZ progenitors upon cKO of cholesterol biosynthesis, we examined the levels of hypoxia-inducible factor-1 (HIF-1), a major inducer of VEGF expression (37, 38). Remarkably, HIF-1α levels in the E13.5 *SQS*-cKO DiE were essentially the same as in control (Fig. 5*D*). Similarly, the mRNA level of the glucose transporter Glut1, a target gene whose expression is known to be stimulated by HIF-1 (38, 39), was also unaltered in the E13.5 DiE upon *SQS* cKO (Fig. 5*E*). Taken together, these data indicate that the upregulation of VEGF expression in VZ progenitors upon cKO of cholesterol biosynthesis occurs via a HIF-1–independent pathway.

Discussion

A key finding of the present study is the demonstration that neural stem cells are able to compensate for the ablation of endogenous cholesterol biosynthesis by upregulating VEGF expression, thereby promoting angiogenesis into the neurogenic niche and consequently increasing their supply with cholesterol-bearing lipoproteins. It has been known that statins, which inhibit 3-hydroxy-3-methylglutaryl coenzyme A reductase and thus the biosynthesis of isoprenoids including cholesterol, can cause an upregulation of VEGF and promote angiogenesis, but these effects have generally been thought to be independent of the cholesterol-lowering function of statins and to involve geranylated proteins as well as nitric oxide and Akt signaling (40–44). In contrast, our approach was to selectively ablate the biosynthesis of cholesterol (rather than that of all isoprenoids), and so the present study establishes a direct link between intracellular cholesterol levels, VEGF expression, and angiogenesis and, importantly, has addressed the relevance of this link for neural stem cells and the development of the mammalian brain.

The increase in lipid droplets observed for the neural stem and progenitor cells as well as their neuronal progeny in the *SQS*-cKO brain presumably reflected an increased uptake of cholesterol-bearing lipoproteins into these cells. The latter was likely due, at least in part, to the elevated lipoprotein supply resulting from the increased angiogenesis, although in the case of the VZ progenitors an increased uptake from the ventricular fluid may also have occurred. Besides cholesterol ester, lipoproteins are known to contain other lipids with unsaturated fatty acyl chains (45), which would explain the increased abundance in the *SQS*-cKO brain of lipid droplets containing TAGs with unsaturated fatty acyl chains.

Considering that *SQS* was ablated in neural stem and progenitor cells, the preferential apoptosis of newborn neurons, resulting in a dramatically smaller brain and lethality at birth, is remarkable. [Although the particular *nestin*-Cre line we used has been reported to result in the ablation of floxed genes selectively in the nervous system (17), we cannot exclude phenotypic effects due to SQS ablation outside the CNS (e.g., in the peripheral nervous system).] This is even more so the case given that it was previously observed that neurons in the adult cerebellum do not require endogenous cholesterol biosynthesis (46). Possible explanations as to why *SQS* exon 5–deficient neurons were so much more sensitive to the lack of endogenous cholesterol biosynthesis than their own mutant progenitors include the following. First, there was no striking upregulation of VEGF expression and no marked increase in angiogenesis in the NL as there was in the VZ, and so compensation via increased lipoprotein supply from the blood circulation may have occurred to a lesser extent in the case of neurons than VZ progenitors. (This explanation is not necessarily contradicted by the lipid droplet increase in the NL, because this could reflect inheritance of these organelles from progenitors.) Second, in contrast to VZ progenitors, neurons do not have direct access to the ventricular fluid, which is known to contain cholesterol-bearing lipoproteins (22), and hence are deprived of this other route of compensation. Third, given the fact that neurons form extensive processes, which implies plasma membrane growth, they may have a greater need for cholesterol than VZ progenitors, in particular during development. Fourth, considering the marked increase in lipid droplets, neurons may be more sensitive to lipotoxicity (47) than VZ progenitors.

In conclusion, the neural stem cells of the mammalian brain are endowed with 2 specific properties that enable them to avoid the detrimental consequences of a lack of endogenous cholesterol. First, by lining the lumen of a cavity filled with lipoproteins (i.e., the neural tube), they are privileged to access a unique source of cholesterol. Second, they can signal to increase their supply with lipoproteins from the blood circulation. As shown in the present study, these 2 features of neural stem cells provide an effective means of compensation that is lacking in their neuronal progeny, resulting in the massive depletion of neurons.

Materials and Methods

Animals. Inactivation of the squalene synthase gene (*SQS*/*Fdft1*) in VZ cells was obtained by crossing *SQS*$^{flox/wt}$/*nestin-Cre*$^{+/-}$ mice with *SQS*$^{flox/flox}$ mice (16, 17). Embryos were genotyped by PCR. *SQS*$^{flox/flox}$/*nestin-Cre*$^{-/-}$ or *SQS*$^{flox/wt}$/*nestin-Cre*$^{-/-}$ mice were used as controls, *SQS*$^{flox/wt}$/*nestin-Cre*$^{+/-}$ mice as heterozygous animals, and *SQS*$^{flox/flox}$/*nestin-Cre*$^{+/-}$ mice as *SQS*-cKO animals. All experiments were performed in accordance with German animal welfare legislation.

Morphologic and Biochemical Analyses. Immunohistochemistry, in situ hybridization, transmission EM, RT-PCR, and immunoblotting were performed according to standard methods, details of which and of the ensuing quantifications are described in *SI Text*. For the determination of blood vessel area, the circumference of all PECAM-1–stained blood vessels in a given image was traced, and the included areas were determined in pixels with Image-J software (National Institutes of Health).

Lipid Extraction and TLC Analysis. Lipids were extracted from E13.5 dTE plus DiE of control, heterozygous, and *SQS*-cKO mice using methanol-chloroform and analyzed by TLC using 2 sequential runs, first in ethanol/chloroform/triethylamine/water 40:35:35:9 (vol/vol/vol/vol) and then in n-hexane/ethylacetate 5:1 (vol/vol), followed by quantification, as is described in detail in *SI Text*.

Mass Spectrometric Analysis. Lipid extracts were analyzed as described previously (48, 49). Briefly, aliquots were diluted 100-fold with chloroform/methanol/2-propanol 1:2:4 (vol/vol/vol) containing 3.5 mM ammonium acetate, vortexed thoroughly, and centrifuged for 2 min at 13,000 $\times$ *g* on a Minispin centrifuge (Eppendorf). Analyses were performed on an LTQ-Orbitrap hybrid mass spectrometer (Thermo Fisher Scientific) equipped with a robotic nanoflow ion source, NanoMate HD (Advion BioSciences). Mass spectrometry survey scans were acquired using the Orbitrap analyzer operated under the target mass resolution of 100,000 (full width at half-maximum defined at *m/z* 400) with automatic gain control set to 5.0×10^5 as target value. Lipids were identified by in-house-developed LipidX software, relying on their accurately determined *m/z* (error <3.5 ppm), which met specific lipid class sum composition constraints.

ACKNOWLEDGMENTS. We thank Jussi Helppi of the animal facility of Max Planck Institute of Molecular Cell Biology and Genetics for excellent support; Svetlana Rylova for MCF-7 lysate; and Drs. Christo Goridis and Temo Kurzchalia for helpful discussion and comments on the manuscript. Supported by a fellowship from the Japan Society for the Promotion of Science (to K.S.), by Grants SFB 655, A8 (to G.B.) and SFB 655, A2 (to W.B.H.) from the Deutsche Forschungsgemeinschaft (DFG), by the DFG-funded Center for Regenerative Therapies Dresden, and by the Fonds der Chemischen Industrie (to W.B.H.).

1. Simons K, Ikonen E (1997) Functional rafts in cell membranes. *Nature* 387:569–572.
2. Brown D, London E (1998) Functions of lipid rafts in biological membranes. *Annu Rev Cell Dev Biol* 14:111–136.
3. Simons K, Vaz WL (2004) Model systems, lipid rafts, and cell membranes. *Annu Rev Biophys Biomol Struct* 33:269–295.
4. Suzuki T (2002) Lipid rafts at postsynaptic sites: Distribution, function and linkage to postsynaptic density. *Neurosci Res* 44:1–9.
5. Ledesma MD, Dotti CG (2005) The conflicting role of brain cholesterol in Alzheimer's disease: Lessons from the brain plasminogen system. *Biochem Soc Symp* 129–138.
6. Kamiguchi H (2006) The region-specific activities of lipid rafts during axon growth and guidance. *J Neurochem* 98:330–335.
7. Guirland C, Zheng JQ (2007) Membrane lipid rafts and their role in axon guidance. *Adv Exp Med Biol* 621:144–155.
8. Mauch DH, et al. (2001) CNS synaptogenesis promoted by glia-derived cholesterol. *Science* 294:1354–1357.
9. Pfrieger FW (2003) Role of cholesterol in synapse formation and function. *Biochim Biophys Acta* 1610:271–280.
10. Tozawa R, et al. (1999) Embryonic lethality and defective neural tube closure in mice lacking squalene synthase. *J Biol Chem* 274:30843–30848.
11. Corbeil D, Röper K, Fargeas CA, Joester A, Huttner WB (2001) Prominin: A story of cholesterol, plasma membrane protrusions and human pathology. *Traffic* 2:82–91.
12. Röper K, Corbeil D, Huttner WB (2000) Retention of prominin in microvilli reveals distinct cholesterol-based lipid microdomains in the apical plasma membrane. *Nat Cell Biol* 2:582–592.
13. Marzesco AM, et al. (2005) Release of extracellular membrane particles carrying the stem cell marker prominin-1 (CD133) from neural progenitors and other epithelial cells. *J Cell Sci* 118:2849–2858.
14. Dubreuil V, Marzesco AM, Corbeil D, Huttner WB, Wilsch-Brauninger M (2007) Midbody and primary cilium of neural progenitors release extracellular membrane particles enriched in the stem cell marker prominin-1. *J Cell Biol* 176:483–495.
15. Marzesco AM, et al. (2009) Release of extracellular membrane vesicles from microvilli of epithelial cells is enhanced by depleting membrane cholesterol. *FEBS Lett* 583:897–902.
16. Saher G, et al. (2005) High cholesterol level is essential for myelin membrane growth. *Nat Neurosci* 8:468–475.
17. Tronche F, et al. (1999) Disruption of the glucocorticoid receptor gene in the nervous system results in reduced anxiety. *Nat Genet* 23:99–103.
18. Graus-Porta D, et al. (2001) Beta1-class integrins regulate the development of laminae and folia in the cerebral and cerebellar cortex. *Neuron* 31:367–379.
19. Caccamo D, et al. (1989) Immunohistochemistry of a spontaneous murine ovarian teratoma with neuroepithelial differentiation. Neuron-associated beta-tubulin as a marker for primitive neuroepithelium. *Lab Invest* 60:390–398.
20. Stadelmann C, Lassmann H (2000) Detection of apoptosis in tissue sections. *Cell Tissue Res* 301:19–31.
21. Lendahl U, Zimmerman LB, McKay RD (1990) CNS stem cells express a new class of intermediate filament protein. *Cell* 60:585–595.
22. Bachy I, Kozyraki R, Wassef M (2008) The particles of the embryonic cerebrospinal fluid: How could they influence brain development? *Brain Res Bull* 75:289–294.
23. Brown DA (2001) Lipid droplets: Proteins floating on a pool of fat. *Curr Biol* 11:R446–R449.
24. Thiele C, Spandl J (2008) Cell biology of lipid droplets. *Curr Opin Cell Biol* 20:378–385.
25. Walther TC, Farese RV, Jr (2009) The life of lipid droplets. *Biochim Biophys Acta*, in press.
26. Olofsson SO, et al. (2009) Lipid droplets as dynamic organelles connecting storage and efflux of lipids. *Biochim Biophys Acta*, in press.
27. Heid HW, Schnolzer M, Keenan TW (1996) Adipocyte differentiation-related protein is secreted into milk as a constituent of milk lipid globule membrane. *Biochem J* 320(Pt 3):1025–1030.
28. Hayat M (2000) *Principle and Techniques of Electron Microscopy: Biological Applications* (Cambridge Univ Press).
29. McCarthy RA, Barth JL, Chintalapudi MR, Knaak C, Argraves WS (2002) Megalin functions as an endocytic sonic hedgehog receptor. *J Biol Chem* 277:25660–25667.
30. May P, Herz J (2003) LDL receptor-related proteins in neurodevelopment. *Traffic* 4:291–301.
31. Assemat E, et al. (2005) Overlapping expression patterns of the multiligand endocytic receptors cubilin and megalin in the CNS, sensory organs and developing epithelia of the rodent embryo. *Gene Expr Patterns* 6:69–78.
32. Woodfin A, Voisin MB, Nourshargh S (2007) PECAM-1: A multi-functional molecule in inflammation and vascular biology. *Arterioscler Thromb Vasc Biol* 27:2514–2523.
33. Breier G, Albrecht U, Sterrer S, Risau W (1992) Expression of vascular endothelial growth factor during embryonic angiogenesis and endothelial cell differentiation. *Development* 114:521–532.
34. Hogan KA, Ambler CA, Chapman DL, Bautch VL (2004) The neural tube patterns vessels developmentally using the VEGF signaling pathway. *Development* 131:1503–1513.
35. Adams RH, Alitalo K (2007) Molecular regulation of angiogenesis and lymphangiogenesis. *Nat Rev Mol Cell Biol* 8:464–478.
36. Ruhrberg C, et al. (2002) Spatially restricted patterning cues provided by heparin-binding VEGF-A control blood vessel branching morphogenesis. *Genes Dev* 16:2684–2698.
37. Pages G, Pouyssegur J (2005) Transcriptional regulation of the Vascular Endothelial Growth Factor gene—a concert of activating factors. *Cardiovasc Res* 65:564–573.
38. Hirota K, Semenza GL (2006) Regulation of angiogenesis by hypoxia-inducible factor 1. *Crit Rev Oncol Hematol* 59:15–26.
39. Kroemer G, Pouyssegur J (2008) Tumor cell metabolism: Cancer's Achilles' heel. *Cancer Cell* 13:472–482.
40. Weis M, Heeschen C, Glassford AJ, Cooke JP (2002) Statins have biphasic effects on angiogenesis. *Circulation* 105:739–745.
41. Skaletz-Rorowski A, Walsh K (2003) Statin therapy and angiogenesis. *Curr Opin Lipidol* 14:599–603.
42. Ma FX, Han ZC (2005) Statins, nitric oxide and neovascularization. *Cardiovasc Drug Rev* 23:281–292.
43. Nakao T, Shiota M, Tatemoto Y, Izumi Y, Iwao H (2007) Pravastatin induces rat aortic endothelial cell proliferation and migration via activation of PI3K/Akt/mTOR/p70 S6 kinase signaling. *J Pharmacol Sci* 105:334–341.
44. Wu H, et al. (2008) Simvastatin-mediated upregulation of VEGF and BDNF, activation of the PI3K/Akt pathway, and increase of neurogenesis are associated with therapeutic improvement after traumatic brain injury. *J Neurotrauma* 25:130–139.
45. Fuchs B, Schiller J (2008) MALDI-TOF MS analysis of lipids from cells, tissues and body fluids. *Subcell Biochem* 49:541–565.
46. Fünfschilling U, Saher G, Xiao L, Mobius W, Nave KA (2007) Survival of adult neurons lacking cholesterol synthesis in vivo. *BMC Neurosci* 8:1.
47. Schaffer JE (2003) Lipotoxicity: When tissues overeat. *Curr Opin Lipidol* 14:281–287.
48. Schwudke D, et al. (2007) Top-down lipidomic screens by multivariate analysis of high-resolution survey mass spectra. *Anal Chem* 79:4083–4093.
49. Grimard V, et al. (2008) siRNA screening reveals JNK2 as an evolutionary conserved regulator of triglyceride homeostasis. *J Lipid Res* 49:2427–2440.